

Probing helical vs chiral character of topological superconductors via non-local Hanbury-Brown and Twiss correlations

Tusaradri Mohapatra, Subhajit Pal and Colin Benjamin*

School of Physical Sciences, National Institute of Science Education & Research, HBNI, Jatni-752050, India

Topological superconductors host surface Andreev bound states which can be classified as chiral or helical. Chiral superconductors belong to Z symmetry class which breaks time-reversal symmetry (TRS) while helical superconductors belong to Z_2 symmetry class which preserves TRS. Chiral and helical superconductors can be further categorized by the parity-even or odd, of their order parameter. In this paper using Hanbury Brown and Twiss (HBT) shot noise correlations and the non-local conductance, we probe metal/unconventional superconductor/metal junctions in order to better understand the pairing helical vs chiral in topological superconductors. We also compare these to non-topological superconductors. Topological superconductors are carriers of Majorana fermions which are important for topological quantum computation. By distinguishing chiral superconductors, wherein Majorana bound states (MBS) persist even in presence of a magnetic field, from helical superconductors where MBS are fragile, our study will help in the search for stable Majorana fermions which will be useful for topological quantum computation.

I. INTRODUCTION

Spin singlet superconductors are s -wave type superconductors with spherically symmetric order parameter wherein pairing potential is independent of direction of incident electrons and any deviation from this is defined as an unconventional superconductor, e.g., p -wave and d -wave [1]. A new class of superconductors has come into being which can host surface Andreev bound states (SABS) known as topological superconductors [2, 3]. Topological superconductors are building blocks of Majorana zero modes which are of potential importance in topological quantum computation [3, 4]. Topological superconductors can be further classified as chiral, i.e., belong to topological symmetry class Z (break time reversal symmetry) or helical which belong to Z_2 topological symmetry class (preserve time reversal symmetry) [5]. In topological superconductors due to change in pairing potential on the Fermi surface, SABS are generated [6]. SABS have an energy(E) dispersion which is linear in momenta(k) for chiral ($E \propto k$) and helical ($E \propto \pm k$). SABS exist in topological superconductors that host Bogoliubov quasiparticles which in this case are massless Majorana fermions [9]. In chiral superconductors, MBS persist even in presence of magnetic field, are robust against strong magnetic field and disorder [8], while MBS seen in helical superconductors are fragile to strong magnetic field and disorder [10–12]. Distinguishing chiral from helical superconductor will be helpful in studying the effect of magnetic fields on topological superconductors.

Among the many proposals to detect the pairing symmetry of topological superconductors, a well known method is nuclear magnetic resonance (NMR) Knight shift measurement [13]. Invariance of the Knight shift to a change in temperature below T_c is strongly suggesting of spin triplet pairing (either chiral- p or helical- p) in topological superconductors [14]. Further, from various studies on Josephson coupling between s -wave and Sr_2RuO_4 superconductors, it has been inferred that Josephson coupling is not allowed along

c axis but allowed along ab plane [15]. This selection rule is again strong evidence that the famous topological superconductor Sr_2RuO_4 is a possible candidate for chiral- p state. Another method, current and magnetic field inversion (CFI) symmetry test of time-reversal symmetry (TRS) can be used as a tool to discriminate between the chiral and helical superconductors. CFI preserves TRS for helical superconductors while it breaks TRS for chiral superconductors [16]. CFI test along with Knight shift measurement can be helpful in discriminating between chiral- p , chiral- d and helical- p pairing in topological superconductors. However, spontaneous magnetic induction at sample edge as expected for chiral- p order parameter was not detected in scanning SQUIDs [18] and scanning hall probe [23] measurements. Origin of these inconsistencies has not been fully resolved and these tests are not 100% full proof, so we propose two additional tests, the non-local conductance and non-local HBT correlations in metal/unconventional superconductor/metal junction to distinguish between topological (chiral- p , chiral- d and helical- p) and non-topological (s , $d_{x^2-y^2}$) superconductors. To decipher the pairing symmetry of unconventional superconductors, quantum transport in superconducting hybrid junctions via measurement of differential conductance has been helpful. However, shot noise or non-local HBT correlations can give more information about Cooper pair splitting which may be helpful in differentiating between pairing symmetries of unconventional superconductors. HBT correlations have been invoked in the context of intensity-intensity correlations of photons received from stars [27]. In Ref. [34], it was seen that negative bias voltage applied in NSN junctions can give different results for shot noise cross-correlation and differential shot noise cross-correlation. Hence, we not only focus on shot noise cross-correlations but extend our study to differential shot noise cross-correlations as well in our setup.

Pairing symmetry of superconductors is classified based on spin angular momentum (S) of Cooper pairs, which form via pairing between two spin half electrons, it can be either singlet (0) or triplet (1). Spin singlet states are asymmetric in spin space while spin triplet states are symmetric. Any pairing symmetry has to have a definite parity under spatial inver-

* colin.nano@gmail.com

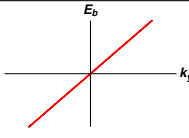
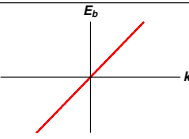
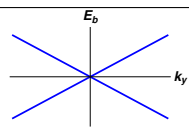
sion. When orbital part of wavefunction is even under spatial inversion it is denoted as even parity with orbital angular momentum ($L = 0, 2, 4, \dots$) while when the orbital part is odd under spatial inversion it is called odd parity with orbital angular momentum ($L = 1, 3, 5, \dots$). Due to Pauli exclusion principle, total wave function of Cooper pair must be asymmetric under exchange of particles. Asymmetric spin singlet pairing corresponds to even orbital angular momentum and symmetric spin triplet pairing corresponds to odd orbital angular momentum [28]. Even parity, spin singlet Cooper pair states with angular momentum $L = 0, 2$ are denoted as s -wave, d -wave while odd parity, spin triplet Cooper pair states with angular momentum $L = 1, 3$ are denoted as p -wave, f -wave.

Sr_2RuO_4 is a good example of chiral spin-triplet p -wave superconductor [24] and $\text{In}_3\text{Cu}_2\text{VO}_9$ and SrPtAs are examples of chiral d -wave superconductors [26]. Pairing potential ($\hat{\Delta}(\mathbf{k})$) of Cooper pair is written in terms of $\mathbf{d}(\mathbf{k})$, with $\hat{\Delta}(\mathbf{k}) = \Delta(\mathbf{d}(\mathbf{k}) \cdot \hat{\sigma}) i \sigma_2$ where $\mathbf{d}(\mathbf{k}) = d_x \hat{x} + d_y \hat{y} + d_z \hat{z}$ and d_x, d_y and d_z are the three components of translational vector, while momenta $\mathbf{k} = k_x \hat{x} + k_y \hat{y} + k_z \hat{z}$, $\hat{\sigma} = \sigma_1 \hat{x} + \sigma_2 \hat{y} + \sigma_3 \hat{z}$ wherein

$\sigma_{1,2,3}$ are three Pauli matrices. For 2D superconductor, momentum components are $k_x = k_F \cos \theta$, $k_y = k_F \sin \theta$ and $k_z = 0$ where k_F is Fermi wave vector and θ is angle the incident electron makes with x axis. In superfluid ^3He and Sr_2RuO_4 spin triplet p wave states can be defined as chiral- p where $\mathbf{d}(\mathbf{k}) = (k_x \pm i k_y) \hat{z} / k_F$ with $\mathbf{d} \parallel \hat{z}$, i.e., \mathbf{d} is parallel to crystal c axis [29], implying, $\mathbf{d}(\mathbf{k}) = (\cos \theta \pm i \sin \theta) \hat{z}$. For chiral d wave superconductor [26], $\mathbf{d}(\mathbf{k}) = (k_x^2 + k_y^2 + i 2 k_x k_y) \hat{z} / k_F = e^{i 2 \theta} \hat{z}$. Anisotropic Sr_2RuO_4 has helical SABS which are spin triplet p wave states. In this case \mathbf{d} can be defined as $(\hat{x} k_x \pm \hat{y} k_y) / k_F$ or $(\hat{x} k_y \pm \hat{y} k_x) / k_F$ with $\mathbf{d} \perp \hat{z}$ (\mathbf{d} in ab plane), i.e., \mathbf{d} is perpendicular to the crystal c axis [29, 42], implying, $\mathbf{d}(\mathbf{k}) = (\hat{x} \cos \theta \pm \hat{y} \sin \theta)$ or $(\hat{x} \sin \theta \pm \hat{y} \cos \theta)$.

Non-topological superconductors are not only of gapful s -wave type but can also be nodal. Examples of non topological nodal superconductors are p_y superconductor [21], e.g. $\text{Ni}_{80}\text{Fe}_{20}$ where the order parameter vanishes in y direction with $\mathbf{d}(\mathbf{k}) = (k_y) \hat{z} / k_F = \sin \theta \hat{z}$ and $d_{x^2-y^2}$ superconductor wherein order parameter vanishes in diagonal of x, y direction of d wave superconductor [22] with $\mathbf{d}(\mathbf{k}) = (k_x^2 - k_y^2) \hat{z} / k_F = \cos 2 \theta \hat{z}$.

Table I: Pairing Symmetry of unconventional superconductors with examples. Plots of surface Andreev bound states (SABS) E_b (in units of Δ) are obtained via the zeros of denominator of scattering amplitudes obtained from solving the Normal Metal-Topological superconductor scattering problem.

Topology	Type	Pairing	Parity	d_x	d_y	d_z	SABS	Examples
Non Topological	Gapful	s	Even	0	0	1	No	Alkali doped fullerenes (A_3C_{60} with $\text{A} = \text{K, Rb, Cs}$)
	Nodal	p_y	Odd	0	0	k_y	No	$\text{Ni}_{80}\text{Fe}_{20}$
		$d_{x^2-y^2}$	Even	0	0	$k_x^2 + k_y^2$	No	$\text{Nd}_{1-x}\text{Sr}_x\text{NiO}_2$
Topological	Chiral (Gapful)	$p_x + i p_y$	Odd	0	0	$k_x + i k_y$		Superfluid ^3He
		$d_{x^2-y^2} + i d_{xy}$	Even	0	0	$k_x^2 + k_y^2 + 2 i k_x k_y$		SrPtAs
	Helical (Gapful)	p	Odd	k_x	k_y	0		Sr_2RuO_4

In Table 1, examples of topological and non-topological superconductors are given with their respective pairing symmetries. Topological gapful superconductors are chiral p -wave which is $p_x + i p_y$ superconductor [24] and chiral d -wave which is $d_{x^2-y^2} + i d_{xy}$ spin singlet superconductor [26]. Topological superconductors exhibit surface Andreev bound states (SABS) whereas in non-topological superconductor SABS are ab-

sent. The calculation of SABS for topological superconductors with bound state energy dispersion as a function of momentum vector k_y is described here in brief. We calculate SABS for normal metal/superconductor junction with chiral p , chiral d and helical p pairing. Presence of SABS is a supporting evidence for topological superconductivity. Differential conductance for normal metal/unconventional supercon-

ductor junction is $G = 1 + |a|^2 - |b|^2$, where a is Andreev reflection amplitude and b is normal reflection amplitude. Denominator of $G \rightarrow 0$ at $E = E_b$, which defines energy E_b of Andreev bound state at surface, which is also known as surface Andreev bound state (SABS). SABS plots for chiral (chiral- p and chiral- d) and helical- p superconductors are given in Table 1. For normal metal/helical- p superconductor junction, denominator of differential conductance G , is equal to zero at $E = E_b$, and for $k_x = 0$ is given as $16(E/\Delta)^2 - 36|k_y|^2 = 0$, or $\frac{E_b}{\Delta} \propto \pm|k_y|$. Similarly, for normal metal/chiral- p superconductor junction, when denominator of differential conductance G is equated to zero we get $E = E_b$, and again for $k_x = 0$ is $\frac{E_b}{\Delta} \propto k_y$. Finally, for normal metal/chiral- d superconductor junction, equating denominator of differential conductance G to zero, for $k_x = 0$, we get $\frac{E_b}{\Delta} \propto k_y$.

The manuscript is organized as follows: the next section, deals with 2D BTK approach and how it is used to calculate HBT noise and non-local conductance for our system. Next, in section III we describe our setup a 2D normal metal(N_1)/insulator(I)/unconventional superconductor(US)/insulator(I)/normal metal(N_2) junction focusing first on Hamiltonian for a non topological US followed by chiral and helical superconductors. Then we discuss the wave functions and boundary conditions which are necessary to calculate non-local conductance, shot noise, i.e., HBT noise correlation and differential shot noise. This is followed by a discussion on results, first for non-local conductance then differential shot noise cross-correlations and HBT shot noise cross correlations and finally on why we see what we see. We finally conclude with a comparison of the different pairing symmetries: helical vs chiral vs. non-topological using HBT noise as well as differential non-local conductance. In appendix, we have elaborated in detail on the components of shot noise cross-correlation. We see that different pairing symmetries can be very effectively distinguished using shot noise cross-correlations (including differential shot noise) and the non-local conductance.

II. 2D BTK APPROACH

We consider a $N_1/I/US/I/N_2$ junction see Fig. 1, with insulators at $x = -R/2$ and $x = R/2$. θ is angle, the incident (transmitted) electrons make with x axis [30] in N_1 (N_2) region. θ_a is angle, reflected (transmitted) holes make with x axis in N_1 (N_2) region. Finally, $\theta_{e(h)}$ is angle, transmitted electrons (holes) make with x axis in US region. We use Andreev approximation throughout this paper which implies that Fermi wave vector (k_F) for both electrons and holes in N_1 or N_2 or US regions remains same. This further implies that $\theta = \theta_a = \theta_{e(h)}$. Due to presence of translational invariance in y direction [31], Fermi wave vectors in N_1 , N_2 and US regions are conserved.

In Fig. 1 Andreev reflection amplitude is denoted as $a = s_{11}^{eh}$, normal reflection amplitude as $b = s_{11}^{ee}$, transmission amplitude of elastic cotunneling $c = s_{12}^{ee}$, transmission amplitude of cross

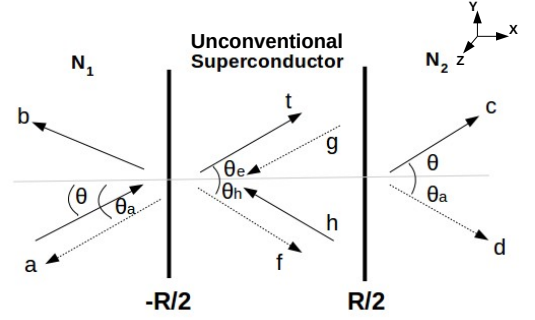


Figure 1: Schematic illustration of reflection and transmission of electron in a normal metal(N_1)/insulator(I)/unconventional superconductor(US)/insulator(I)/normal metal(N_2) junction in $x-y$ plane. Solid line represent scattering of electrons while the dotted line represent scattering of holes.

Andreev reflection $d = s_{12}^{eh}$. Scattering amplitude $s_{ik}^{\alpha\gamma}$ represents a particle α ($\in e, h$) incident from contact i ($\in N_1, N_2$) which is reflected or transmitted to contact k ($\in N_1, N_2$) as a particle γ ($\in e, h$). In Fig. 2 we show our chosen setting to study transport and current cross correlations across unconventional superconductors for a 2D $N_1/I/US/I/N_2$ junction wherein N_1 is at bias voltage V_1 and N_2 is at bias voltage V_2 while US is grounded.

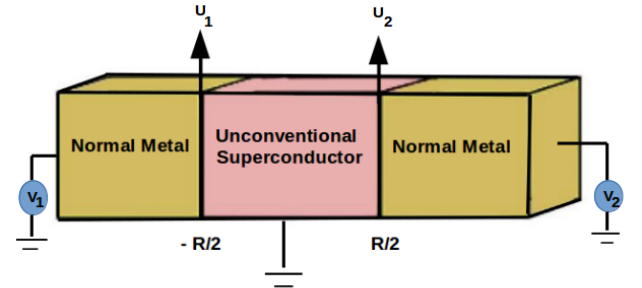


Figure 2: 2D $N_1/I/US/I/N_2$ junction. The superconductor is grounded while bias voltages V_1 is applied to N_1 and V_2 is applied to N_2 .

A. Non-local conductance and shot noise

Andreev reflection can be non-local too, which is known as cross Andreev reflection(CAR), in which electron is transmitted as a hole through the other interface with superconductor. This CAR can be considered as the reverse process of splitting of Cooper pair, i.e., spatially separated entangled electrons in either of normal metals.

First, we calculate non-local differential conductance which is defined as conductance in N_2 when both N_2 and US are grounded and voltage is applied to N_1 . The difference be-

tween CAR and elastic cotunneling(EC) in absence of any voltage bias to N_2 is defined as non-local differential conductance [33], $G_{NL} = G_{CAR} - G_{EC}$, where

$$G_{CAR} = \int_{-\pi/2}^{\pi/2} d\theta \frac{\cos\theta}{2\pi} |d|^2, \quad G_{EC} = \int_{-\pi/2}^{\pi/2} d\theta \frac{\cos\theta}{2\pi} |c|^2, \quad (1)$$

$d = s_{12}^{eh}$ is scattering amplitude for CAR while $c = s_{12}^{ee}$ is scattering amplitude for EC. Shot noise can give more details about pairing symmetry from current cross-correlations in the $N_1/I/US/I/N_2$ junction that conductance cannot. This is why we look at shot noise cross-correlation and differential shot noise cross-correlation in the $N_1/I/US/I/N_2$ junction. Discreteness of charge leads to non-equilibrium temporal fluctuations in the current known as shot noise. Even at zero temperature shot noise exists, unlike thermal noise that originates due to finite temperature and vanishes at zero temperature.

The general result for shot noise cross correlation for 2D BTK includes an integral over incident angle θ and is given [35] as,

$$S_{12} = \frac{2e^2}{h} \int_{-\pi/2}^{\pi/2} d\theta \frac{\cos\theta}{2\pi} \sum_{k,l \in 1,2,x,y,\gamma,\delta \in e,h} \text{sgn}(x)\text{sgn}(y) \int dE W_{k,\gamma;l,\delta}(1x,E) W_{l,\delta;k,\gamma}(2y,E) f_{k\gamma}(E) [1 - f_{l\delta}(E)], \quad (2)$$

where parameter $W_{k,\gamma;l,\delta}(1x,E) = \delta_{1k} \delta_{1l} \delta_{x\gamma} \delta_{x\delta} - s_{1k}^{xy*}(E) s_{1l}^{x\delta}(E)$ contains information about the scattering process. $s_{1k}^{xy}(E)$ represents scattering amplitude, with γ denoting an electron or hole incident from contact k which is transmitted to N_1 as particle of type x . $f_{k\gamma}$ is Fermi function for particle of type γ in contact k . Normal metal N_1 is contact 1 while normal metal N_2 is contact 2. Here $\text{sgn}(x) = +1$ for $x = e$, i.e., electron and $\text{sgn}(x) = -1$ for $x = h$, i.e., hole. In a previous study [34] it was shown that sign of shot noise cross-correlation and sign of differential shot noise cross-correlation can be different for some regime of bias voltages applied. Taking cue from this we study both shot noise cross-correlation and differential shot noise cross-correlation. This will be useful in understanding different pairing symmetries in our setup. The differential shot noise cross-correlations $\frac{dS_{12}}{dV}$ in symmetric setup ($V_1 = V_2 = V$) at zero temperature is given as [34, 35],

$$\frac{dS_{12}(V_1 = V_2 = V)}{dV} = \frac{4|e|^3}{h} \text{sgn}(|e|V) \int_{-\pi/2}^{\pi/2} d\theta \frac{\cos\theta}{2\pi} (-s_1 + s_2), \quad (3)$$

where $s_1 = s_a(|e|V) + s_a(-|e|V) + s_b(|e|V) + s_b(-|e|V) + s_c(|e|V) + s_c(-|e|V) + s_d(|e|V) + s_d(-|e|V)$, and $s_2 = s_e(|e|V) + s_e(-|e|V) + s_f(|e|V) + s_f(-|e|V) + s_g(|e|V) + s_g(-|e|V) + s_h(|e|V) + s_h(-|e|V)$ with $s_a = s_{21}^{eh} s_{12}^{he} s_{11}^{hh*} s_{22}^{ee*} + s_{12}^{eh} s_{21}^{he} s_{11}^{ee*} s_{22}^{hh*}$, $s_b = s_{12}^{hh} s_{21}^{ee} s_{11}^{eh*} s_{22}^{he*} + s_{12}^{ee} s_{21}^{hh} s_{11}^{eh*} s_{22}^{he*}$, $s_c = s_{11}^{hh} s_{21}^{ee} s_{11}^{eh*} s_{22}^{he*} + s_{11}^{ee} s_{21}^{hh} s_{11}^{eh*} s_{22}^{he*}$, $s_d = s_{12}^{eh} s_{21}^{he} s_{11}^{hh*} s_{22}^{ee*} + s_{12}^{ee} s_{21}^{hh} s_{11}^{eh*} s_{22}^{hh*}$, $s_e = s_{12}^{ee} s_{21}^{hh} s_{11}^{eh*} s_{22}^{hh*} + s_{12}^{hh} s_{21}^{ee} s_{11}^{eh*} s_{22}^{he*}$, $s_f = s_{12}^{eh} s_{21}^{he} s_{11}^{hh*} s_{22}^{ee*} + s_{12}^{ee} s_{21}^{hh} s_{11}^{eh*} s_{22}^{hh*}$, $s_g = s_{11}^{ee} s_{21}^{hh} s_{11}^{eh*} s_{22}^{hh*} + s_{11}^{hh} s_{21}^{ee} s_{11}^{eh*} s_{22}^{he*}$, $s_h = s_{12}^{ee} s_{21}^{hh} s_{11}^{eh*} s_{22}^{hh*} + s_{12}^{hh} s_{21}^{ee} s_{11}^{eh*} s_{22}^{he*}$.

The differential shot noise cross-correlation in non-local setup at zero temperature with bias voltage $V_1 = V$ applied to N_1 while N_2 grounded is given by,

$$\frac{dS_{12}(V_1 = V, V_2 = 0)}{dV} = \frac{4|e|^3}{h} \text{sgn}(|e|V) \int_{-\pi/2}^{\pi/2} d\theta \frac{\cos\theta}{2\pi} (-s_3 + s_4), \quad (4)$$

where $s_3 = s_m(-|e|V) + s_n(|e|V) + s_c(|e|V) + s_c(-|e|V) + s_i(|e|V) + s_j(-|e|V)$, and $s_4 = s_e(|e|V) + s_g(|e|V) + s_g(-|e|V) + s_k(|e|V) + s_l(-|e|V) + s_f(-|e|V)$, with $s_m = s_{21}^{eh} s_{12}^{he} s_{11}^{hh*} s_{22}^{ee*} + s_{12}^{eh} s_{21}^{he} s_{11}^{ee*} s_{22}^{hh*}$, $s_n = s_{12}^{hh} s_{21}^{ee} s_{11}^{eh*} s_{22}^{he*} + s_{12}^{ee} s_{21}^{hh} s_{11}^{eh*} s_{22}^{he*}$, $s_i = s_{12}^{eh} s_{21}^{he} s_{11}^{hh*} s_{22}^{ee*} + s_{12}^{ee} s_{21}^{hh} s_{11}^{eh*} s_{22}^{hh*}$, $s_j = s_{12}^{eh} s_{21}^{he} s_{11}^{hh*} s_{22}^{ee*} + s_{12}^{ee} s_{21}^{hh} s_{11}^{eh*} s_{22}^{hh*}$, $s_k = s_{12}^{ee} s_{21}^{hh} s_{11}^{eh*} s_{22}^{hh*} + s_{12}^{hh} s_{21}^{ee} s_{11}^{eh*} s_{22}^{he*}$, $s_l = s_{12}^{hh} s_{21}^{ee} s_{11}^{eh*} s_{22}^{he*} + s_{12}^{ee} s_{21}^{hh} s_{11}^{eh*} s_{22}^{hh*}$.

The non local conductance and shot noise results for normal incidence ($\theta = 0$) agree with 1D BTK results [32]. In the next section we write wave functions and boundary conditions for $N_1/I/US/I/N_2$ junctions for non-topological superconductors followed by chiral and helical superconductors.

III. THEORY

A. Non-topological superconductor

We adopt Bogoliubov-de Gennes (BDG) approach to study transport in $N_1/I/US/I/N_2$ junction. Hamiltonian for BDG equation [22, 46] $\tilde{H}\psi = E\psi$, with $\tilde{H} = H_0 + \hat{\Delta}(\mathbf{k}, x)$, where

$$H_0 = \begin{pmatrix} H(\mathbf{k}, x) & 0 \\ 0 & -H^*(-\mathbf{k}, x) \end{pmatrix}, \quad (5)$$

with $H(\mathbf{k}, x) = -\frac{\hbar^2 \mathbf{k}^2}{2m} + U(x) - E_F$, and $\mathbf{k} = (k_{x\pm}, k_{y\pm}, 0) = (k_x(\theta_{\pm}), k_y(\theta_{\pm}), 0)$ with $\theta_+ = \theta$ and $\theta_- = \pi - \theta$, $k_x = k_F \cos\theta$ and $k_y = k_F \sin\theta$. $U(x)$, the usual static potential and excitation energy E is measured relative to Fermi energy E_F and m is mass of electron like or hole like quasiparticle. For simplicity, we neglect self-consistency of the spatial distribution of the pair potential in US. The energy gap matrix is,

$$\hat{\Delta}(\mathbf{k}, x) = \Delta(\mathbf{d}(\mathbf{k}), \hat{\sigma}) i\sigma_z \Theta(x - R/2) \Theta(x + R/2), \\ = \Delta \begin{pmatrix} -d_x + id_y & d_z \\ d_z & d_x + id_y \end{pmatrix} \Theta(x - R/2) \Theta(x + R/2), \quad (6)$$

where Θ is Heaviside theta function and d_x , d_y and d_z , three components of translational vector $\mathbf{d}(\mathbf{k})$ which are defined in Table 1 and Δ being magnitude of superconducting gap. $N_1/I/US/I/N_2$ junction has two insulators at $x = -R/2$ and $x = R/2$ described by δ -function potentials: $U(x) = U_1 \delta(x + R/2) + U_2 \delta(x - R/2)$ with U_1 and U_2 being the barrier strengths and R is the thickness of the US. The wave functions in N_1 , non topological US and N_2 regions, for an electron incident from N_1 are

$$\begin{aligned}
\psi_{N_1}(x) &= e^{ik_F y \sin \theta} \left[\begin{pmatrix} 1 \\ 0 \end{pmatrix} (e^{ik_F x \cos \theta} + b e^{-ik_F x \cos \theta}) + a \begin{pmatrix} 0 \\ 1 \end{pmatrix} e^{ik_F x \cos \theta} \right], \text{ for } x < -R/2, \\
\psi_{US}(x) &= e^{ik_F y \sin \theta} \left[\begin{pmatrix} u_+ \\ v_+ \end{pmatrix} t e^{ik_F(x+R/2) \cos \theta} e^{-(x+R/2)/\xi} + \begin{pmatrix} v_- \\ u_- \end{pmatrix} f e^{-ik_F(x+R/2) \cos \theta} e^{-(x+R/2)/\xi} \right. \\
&\quad \left. + \begin{pmatrix} u_- \\ v_- \end{pmatrix} g e^{-ik_F(x-R/2) \cos \theta} e^{(x-R/2)/\xi} + \begin{pmatrix} v_+ \\ u_+ \end{pmatrix} h e^{ik_F(x-R/2) \cos \theta} e^{(x-R/2)/\xi} \right], \text{ for } -R/2 < x < R/2 \text{ and,} \\
\psi_{N_2}(x) &= e^{ik_F y \sin \theta} \left[c \begin{pmatrix} 1 \\ 0 \end{pmatrix} e^{ik_F(x-R/2) \cos \theta} + d \begin{pmatrix} 0 \\ 1 \end{pmatrix} e^{-ik_F(x-R/2) \cos \theta} \right], \text{ for } x > R/2.
\end{aligned} \tag{7}$$

In Eq. 7, coherence factors for electron (hole) quasiparticles are $u_{\pm}(v_{\pm}) = u(\theta_{\pm})(v(\theta_{\pm})) = \sqrt{(E + (-)\sqrt{E^2 - |\Delta_{\pm}|^2})/2E}$ where $\Delta_{\pm} = \Delta(\theta_{\pm})$. From Eq. 5, for a non topological gapful s wave superconductor, $\Delta(\theta_{\pm}) = \Delta$. For non topological nodal p_y wave superconductor, pair potential is $\Delta(\theta_{\pm}) = \Delta \sin(\theta_{\pm}) = \Delta \sin(\theta)$. Finally, for non-topological nodal $d_{x^2-y^2}$ wave superconductor $\Delta(\theta_{\pm}) = \Delta \cos(2\theta_{\pm}) = \Delta \cos(2\theta)$. BCS coherence length $\xi = \hbar v_F / \Delta$ where v_F is the Fermi velocity [40].

B. Topological superconductor

In this subsection we express the wave functions for chiral superconductors followed by helical- p wave superconductor.

1. Chiral superconductors

Hamiltonian for a $N_1/I/US/I/N_2$ set up with chiral pairing symmetry is given as $\hat{H}\psi = E\psi$ with $\hat{H} = H_0 + s_{\sigma}\hat{\Delta}(\mathbf{k}, x)$, where H_0 is defined as in Eq. 5 and $s_{\sigma} = (-1)^{\sigma-1}$ with $\sigma = 1(2)$ labeling for spin-up(down) quasiparticles. Wave functions in N_1 , US with chiral pairing symmetry and N_2 regions, for an electron incident from N_1 are,

$$\begin{aligned}
\psi_{N_1}(x) &= e^{ik_F y \sin \theta} \left[\begin{pmatrix} 1 \\ 0 \end{pmatrix} (e^{ik_F x \cos \theta} + b_{\sigma} e^{-ik_F x \cos \theta}) + a_{\sigma} \begin{pmatrix} 0 \\ 1 \end{pmatrix} e^{ik_F x \cos \theta} \right], \text{ for } x < -R/2, \\
\psi_{US(chiral)}(x) &= e^{ik_F y \sin \theta} \left[\begin{pmatrix} u_{\sigma}(\theta) \\ \eta_{\sigma}^*(\theta) v_{\sigma}(\theta) \end{pmatrix} t_{\sigma} e^{ik_F(x+R/2) \cos \theta} e^{-(x+R/2)/\xi} + \begin{pmatrix} \eta_{\sigma}(\theta) v_{\sigma}(\theta) \\ u_{\sigma}(\theta) \end{pmatrix} f_{\sigma} e^{-ik_F(x+R/2) \cos \theta} e^{-(x+R/2)/\xi} \right. \\
&\quad \left. + \begin{pmatrix} u_{\sigma}(\theta_-) \\ \eta_{\sigma}^*(\theta_-) v_{\sigma}(\theta_-) \end{pmatrix} g_{\sigma} e^{-ik_F(x-R/2) \cos \theta} e^{(x-R/2)/\xi} + \begin{pmatrix} \eta_{\sigma}(\theta_-) v_{\sigma}(\theta_-) \\ u_{\sigma}(\theta_-) \end{pmatrix} h_{\sigma} e^{ik_F(x-R/2) \cos \theta} e^{(x-R/2)/\xi} \right], \text{ for } -R/2 < x < R/2, \text{ and} \\
\psi_{N_2}(x) &= e^{ik_F y \sin \theta} \left[c_{\sigma} \begin{pmatrix} 1 \\ 0 \end{pmatrix} e^{ik_F(x-R/2) \cos \theta} + d_{\sigma} \begin{pmatrix} 0 \\ 1 \end{pmatrix} e^{-ik_F(x-R/2) \cos \theta} \right], \text{ for } x > R/2, \tag{8}
\end{aligned}$$

where $\eta_{\sigma}(\theta_{\pm}) = s_{\sigma} \Delta_{\sigma}(\theta_{\pm}) / |\Delta_{\sigma}(\theta_{\pm})|$ where $\theta_+ = \theta$ and $\theta_- = \pi - \theta$. For chiral- p superconductor [41], pair potentials seen by spin-up(down) quasiparticles are $\Delta_{1(2)}(\theta) = +(-)\Delta e^{i\theta}$. For chiral- d superconductor, pair potentials seen by spin-up(down) quasiparticles are $\Delta_{1(2)}(\theta) = +(-)\Delta e^{2i\theta}$. The BCS coherence factors are $u_{\sigma}(\theta_{\pm}) = \sqrt{(E + \sqrt{E^2 - |\Delta_{\sigma}(\theta_{\pm})|^2})/(2E)}$ and $v_{\sigma}(\theta_{\pm}) = \sqrt{(E - \sqrt{E^2 - |\Delta_{\sigma}(\theta_{\pm})|^2})/(2E)}$.

2. Helical- p superconductor

Hamiltonian for a $N_1/I/US/I/N_2$ set up with helical pairing symmetry is given as $\hat{H}\psi = E\psi$ with $\hat{H} = H_0 + \hat{\Delta}(\mathbf{k}, x)$, where H_0 is defined as in Eq. 5. Wave functions in N_1 , US with helical pairing symmetry and N_2 regions, for an electron incident from N_1 are,

$$\begin{aligned}
\psi_{N_1}(x) &= e^{ik_F y \sin \theta} \begin{bmatrix} 1 \\ 0 \end{bmatrix} (e^{ik_F x \cos \theta} + b_\sigma e^{-ik_F x \cos \theta}) + a_\sigma \begin{bmatrix} 0 \\ 1 \end{bmatrix} e^{ik_F x \cos \theta}, \text{ for } x < -R/2, \\
\psi_{US(\text{helical-}p)}(x) &= e^{ik_F y \sin \theta} \begin{bmatrix} u \\ \eta^*(\theta)v \end{bmatrix} t_\sigma e^{ik_F(x+R/2)\cos\theta} e^{-(x+R/2)/\xi} + \begin{bmatrix} -\eta(\theta)v \\ u \end{bmatrix} f_\sigma e^{-ik_F(x+R/2)\cos\theta} e^{-(x+R/2)/\xi} \\
&+ \begin{bmatrix} u \\ \eta^*(\theta_-)v \end{bmatrix} g_\sigma e^{-ik_F(x-R/2)\cos\theta} e^{(x-R/2)/\xi} + \begin{bmatrix} -\eta(\theta_-)v \\ u \end{bmatrix} h_\sigma e^{ik_F(x-R/2)\cos\theta} e^{(x-R/2)/\xi}, \text{ for } -R/2 < x < R/2, \text{ and} \\
\psi_{N_2}(x) &= e^{ik_F y \sin \theta} \begin{bmatrix} 1 \\ 0 \end{bmatrix} c_\sigma e^{ik_F(x-R/2)\cos\theta} + d_\sigma \begin{bmatrix} 0 \\ 1 \end{bmatrix} e^{-ik_F(x-R/2)\cos\theta}, \text{ for } x > R/2,
\end{aligned} \tag{9}$$

where $\sigma = 1(2)$ labels spin-up (down) quasiparticles. BCS coherence factors are $u(v) = \sqrt{(E + (-)\sqrt{E^2 - \Delta^2})/(2E)}$. For helical- p superconductor [42], $\eta(\theta) = (d_x(\theta) + id_y(\theta))/|\mathbf{d}(\theta)|$

with $\mathbf{d}(\theta) = k_F(\cos \theta, \sin \theta, 0)$.

C. Boundary conditions

The general boundary conditions at the interfaces of a $N_1/I/US/I/N_2$ junction at $x = -R/2$ and $R/2$ are given by

$$\begin{aligned}
\Psi_{N_1}|_{x=-R/2} &= \Psi_{N_2}|_{x=-R/2}, \quad \frac{\partial}{\partial x}(\Psi_{US} - \Psi_{N_1})|_{x=-R/2} = (2mU_1/\hbar^2)\Psi_{N_1}|_{x=-R/2}, \\
\Psi_{US}|_{x=R/2} &= \Psi_{N_2}|_{x=R/2}, \quad \frac{\partial}{\partial x}(\Psi_{N_2} - \Psi_{US})|_{x=R/2} = (2mU_2/\hbar^2)\Psi_{US}|_{x=R/2}.
\end{aligned} \tag{10}$$

The barrier strength at the interface are characterized by dimensionless parameters $z_i = 2mU_i/k_F, i = 1, 2$. From the scattering amplitudes $a = s_{11}^{eh}, b = s_{11}^{ee}, c = s_{12}^{ee}, d = s_{12}^{eh}$, we obtain Andreev and normal reflection probabilities as $A = |a|^2$ and $B = |b|^2$. $C = |c|^2$ and $D = |d|^2$ define probabilities for electron co-tunneling (EC) and crossed Andreev reflection (CAR) respectively. Throughout this paper, we consider interface barrier strengths $z = z_1 = z_2$.

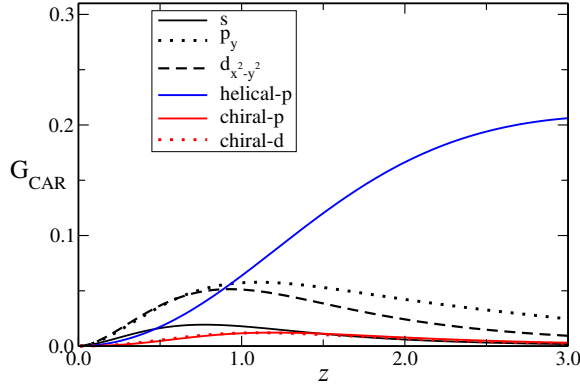
IV. RESULTS AND DISCUSSION

Herein, we calculate differential crossed Andreev conductance G_{CAR} , differential electron co-tunneling conductance G_{EC} , differential non-local conductance G_{NL} , differential shot noise cross-correlations as well as shot noise cross-correlations for $N_1/I/US/I/N_2$ set up as shown in Fig. 2. We take two cases for bias voltages applied in N_1 and N_2 , i.e., $V_1 = V_2$ (symmetric set up) and $V_1 \neq 0, V_2 = 0$ (non-local set up). We plot non local conductance [43, 44] and differential shot noise with the propagating phase $k_F R = 100$ and length of the superconductor in terms of superconducting coherence length $R/\xi = 2$. The reason we take these values for propagating phase $k_F R$ and length of the superconductor is because when $R \gg \xi$, there will be no possibility of non-local transport, as electron like and hole like quasiparticles cannot transmit to the normal metal N_2 . Further, when $R \ll \xi$, the effect of US will be suppressed. How-

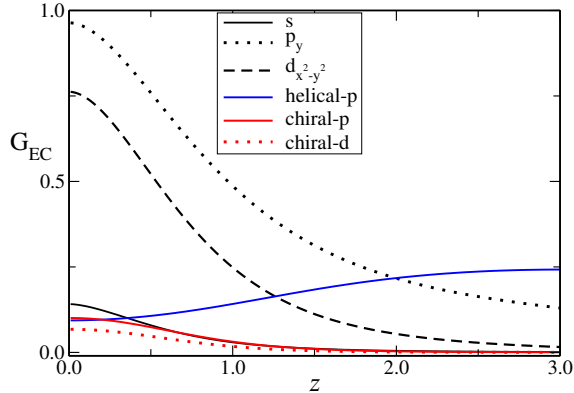
ever, when length of superconductor R is comparable to BCS coherence length ξ , incident quasiparticles can transmit to normal metal N_2 as electron(EC) or hole(CAR). From Refs. [36, 37], one sees a wide range for the propagating phase ($k_F R = 10 - 5000$). It has also been shown that non-local transport will be suppressed for small values [47] of $k_F R$. In chiral- p superconductor (Sr_2RuO_4) [48], BCS coherence length $\xi = 91\text{nm}$ and superconducting gap $\Delta = 1.76 k_B T_c$, where k_B is Boltzmann constant and critical temperature $T_c = 1.6\text{ K}$. Thus, we get a value for Fermi wave vector $k_F = 3 \times 10^8 \text{m}^{-1}$. In this paper we take the length of US, $R = 2\xi$. This gives us, value for propagating phase $k_F R \approx 55$. In this work, we take $k_F R$ to be 100, which is almost in the same range for the veritable topological superconductor (Sr_2RuO_4).

A. Differential non-local conductance (G_{NL})

In Fig. 3, we plot G_{CAR} and G_{EC} vs. barrier strength(z) for non-local set up with $eV_1/\Delta = 0.2, eV_2/\Delta = 0.0$. In Fig. 3a, G_{CAR} for helical- p superconductor tends to finite value in tunnel limit, while for other cases tends to zero. In Fig. 3b G_{EC} for helical- p superconductor tends to finite value but G_{EC} for chiral- p , chiral- d and non-topological superconductors tend to zero in the tunnel limit ($z \rightarrow \text{large}$). For the transparent limit, G_{CAR} for all superconductors is zero while G_{EC} is finite. But it is also quite evident that, G_{NL} is always dominated by G_{EC} .



(a)



(b)

Figure 3: (a) Crossed Andreev conductance G_{CAR} and (b) elastic cotunneling G_{EC} for $N_1/I/US/I/N_2$ junction vs barrier strength (z) for US with different pairing symmetries with $k_F R = 100$, $R/\xi = 2$, $eV_1/\Delta = 0.2$ and $eV_2/\Delta = 0$.

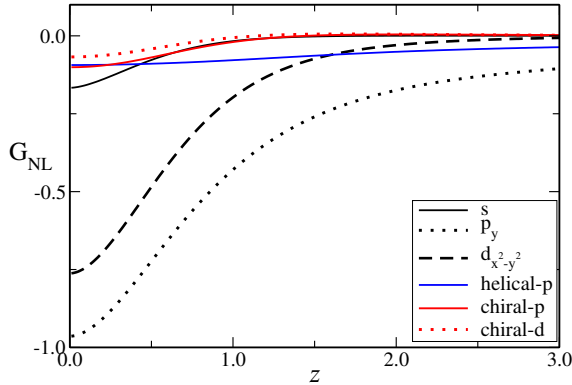


Figure 4: G_{NL} for $N_1/I/US/I/N_2$ junction vs barrier strength (z) for US with different pairing symmetries where $k_F R = 100$, $R/\xi = 2$, $eV_1/\Delta = 0.2$ and $eV_2/\Delta = 0$.

In Fig. 4, we plot G_{NL} vs. z in non-local set up with $eV_1/\Delta =$

0.2, $eV_2/\Delta = 0.0$. G_{NL} for nodal non topological superconductors (p_y and $d_{x^2-y^2}$) is larger in magnitude than gapful non topological(s) and topological superconductors(chiral-p, chiral-d and helical-p) in the transparent limit ($z \rightarrow 0$). G_{NL} for all pairings, tends to zero in the tunnel limit ($z \rightarrow$ large). One doesn't see any marked difference between topological and non-topological superconductors from the non-local conductance. This is because the electron co-tunneling conductance dominates the crossed Andreev conductance. However, one can clearly see that crossed Andreev conductance clearly distinguishes helical-p pairing from the rest. In Fig. 5 we plot

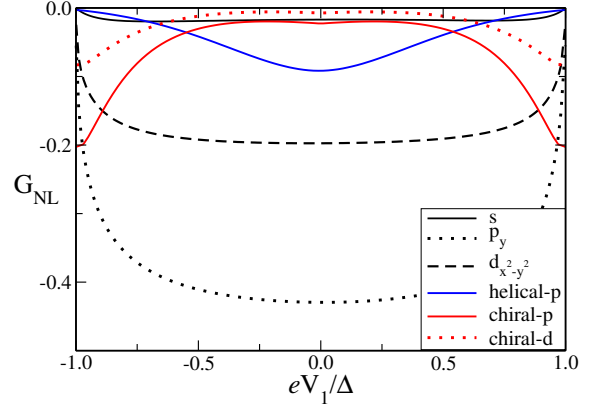


Figure 5: G_{NL} for $N_1/I/US/I/N_2$ junction vs bias voltage (eV_1/Δ) for US with different pairing symmetries where $k_F R = 100$, $R/\xi = 2$, $z = 1$ and $eV_2/\Delta = 0$.

G_{NL} vs. bias voltage (eV_1) with $eV_2/\Delta = 0.0$ for intermediate barrier strength ($z = 1$). G_{NL} , irrespective of pairing is negative for entire range of bias voltage ($-1 < eV_1/\Delta < 1$). However, G_{NL} for chiral superconductors shows a zero bias dip while for helical-p superconductors shows a zero bias peak. When $eV_1 \rightarrow \pm\Delta$, G_{NL} for helical-p and non-topological superconductors vanishes but for chiral superconductors tends to finite negative value. We have also checked that small changes to $k_F R$ and R/ξ does not affect G_{NL} .

B. Differential shot noise cross-correlations

In Fig. 6 we plot differential shot noise cross-correlation vs z for symmetric set up with $eV_1/\Delta = eV_2/\Delta = 0.2$. Differential shot noise cross-correlation for helical-p pairing is negative in transparent limit ($z \rightarrow 0$) while for non-topological and chiral superconductors it is positive. Differential shot noise cross-correlation for helical-p pairing in tunnel limit ($z \rightarrow$ large) tends to positive finite value while for non-topological and chiral pairing vanishes. Differential shot noise cross-correlation for helical-p pairing changes sign from negative to positive with increase in z while for other cases there is no sign change. Thus, differential shot noise cross-correlation can be a good indicator for helical-p pairing symmetry. In Fig. 7 we plot differential shot noise cross-correlation vs z for

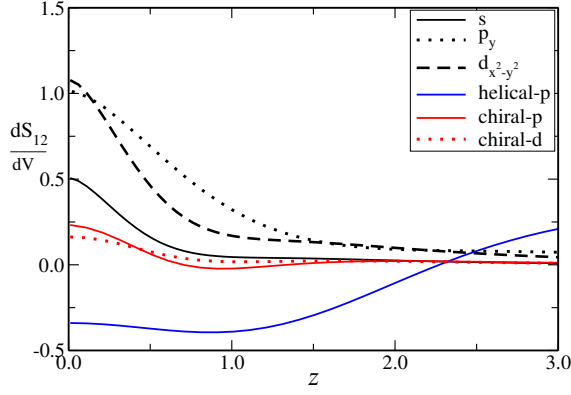


Figure 6: Differential shot noise cross-correlation (symmetric setup, see Eq. 3) in units of $4|e|^3/h$ for $N_1/I/US/I/N_2$ junction vs barrier strength (z), with different pairing symmetries where $k_F R = 100$, $R/\xi = 2$, $eV_1/\Delta = eV_2/\Delta = 0.2$.

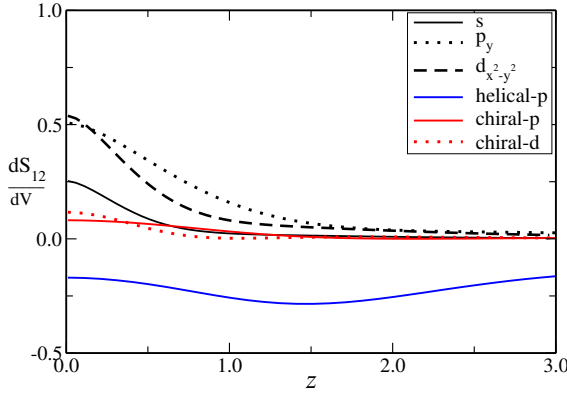


Figure 7: Differential shot noise cross-correlation (non-local setup, see Eq. 4) in units of $4|e|^3/h$ for $N_1/I/US/I/N_2$ junction vs barrier strength (z) for different pairing symmetries of the unconventional superconductor, with $k_F R = 100$, $R/\xi = 2$, $eV_1/\Delta = 0.2$ and $eV_2/\Delta = 0$.

non-local set up with $eV_1/\Delta = 0.2$ and $eV_2/\Delta = 0.0$. Differential shot noise cross correlation for helical- p pairing is negative for entire range of z ($0 < z < 3.5$), but it is positive for both non-topological as well as chiral superconductors for entire range of z . Thus, using differential shot noise cross correlation helical- p superconductor can be easily distinguished from other superconductors.

In Fig. 8 we plot differential shot noise cross-correlation vs bias voltage (eV_1/Δ) in symmetric set up, $eV_2 = eV_1$ and for intermediate barrier strength ($z = 1$). Differential shot noise cross-correlation for helical- p pairing is negative for entire range of bias voltage ($-1 < eV_1/\Delta < 1$) and shows a zero bias peak (ZBP) while for chiral- d superconductor is negative too but shows a zero bias dip (ZBD). However, for chiral- d pairing, differential shot noise cross-correlation turns positive around zero bias. At zero bias, differential shot noise cross-

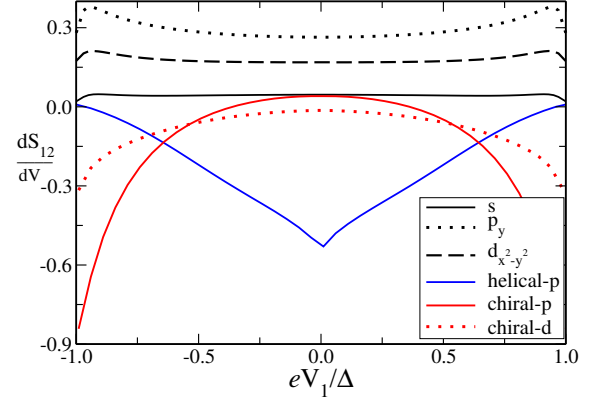


Figure 8: Differential shot noise cross-correlation (for symmetric setup) in units of $4|e|^3/h$ for $N_1/I/US/I/N_2$ junction vs bias voltage (eV_1/Δ) for different pairing symmetries of the unconventional superconductor, with $k_F R = 100$, $R/\xi = 2$, $eV_1 = eV_2$ and $z = 1$.

correlation for non-topological superconductors, gapful(s) as well as nodal(p_y and $d_{x^2-y^2}$) has a finite positive value for entire range of bias voltage ($-1 < eV_1/\Delta < 1$). When $eV_1 \rightarrow \pm\Delta$, differential shot noise cross-correlation for helical- p pairing vanishes while for chiral superconductors (both p and d) tends to finite negative value. When $eV_1 \rightarrow \pm\Delta$, differential shot noise cross-correlation for non-topological gapful superconductor (s) vanishes but for nodal non-topological superconductors (p_y and $d_{x^2-y^2}$) tends to finite positive value. In

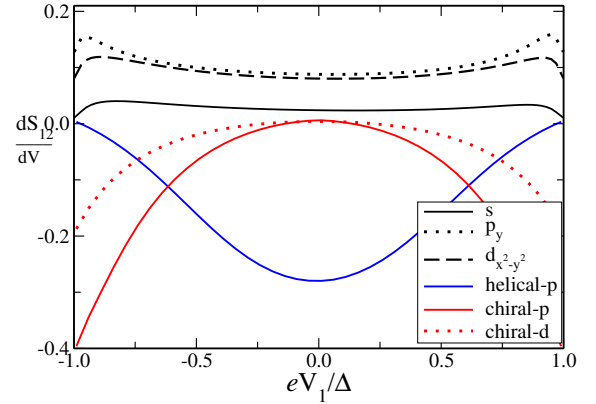


Figure 9: Differential shot noise cross-correlation (for non-local setup) in units of $4|e|^3/h$ for $N_1/I/US/I/N_2$ junction vs bias voltage (eV_1/Δ) for different pairing symmetries with $k_F R = 100$, $R/\xi = 2$, $eV_2/\Delta = 0$ and $z = 1$.

Fig. 9 we plot differential shot noise cross-correlation vs bias voltage (eV_1/Δ) for non-local set up with $eV_2/\Delta = 0.0$ and for intermediate barrier strength ($z = 1$). Differential shot noise cross-correlation for helical- p pairing, similar to symmetric set up, is negative for entire range of bias voltage ($-1 < eV_1/\Delta < 1$) and shows a ZBP while for chiral super-

conductors is again negative for entire range of bias voltage with ZBD. Differential shot noise cross-correlation for non-topological superconductors regardless of pairing is positive for entire range of bias voltage. When $eV_1 \rightarrow \pm\Delta$, differential shot noise cross-correlation for helical- p pairing vanishes while for chiral superconductors tends to a finite negative value. One can clearly see, in both symmetric as well as non-local set up, differential shot noise cross-correlation for helical- p superconductors is negative for entire range of bias voltage while for non-topological superconductor is positive for entire range of bias voltage. Further, while differential shot noise cross-correlation for chiral superconductors in non-local set up is completely negative for entire range of bias voltage. In symmetric setup, differential shot noise cross-correlation for chiral- p pairing may turn positive around zero bias. In Table II we summarize the results for non-local conductance and differential shot noise (in both symmetric and non-local setups). Table II, succinctly puts all results in perspective.

C. Shot noise cross-correlation

Shot noise cross-correlation for our setup (Fig. 2) is calculated using Eq. 2 and plotted as function of bias voltage eV_2/Δ applied to normal metal N_2 for both transparent ($z = 0.1$) junction, see Fig. 10, and for tunnel limit ($z = 3$) in Fig. 11.

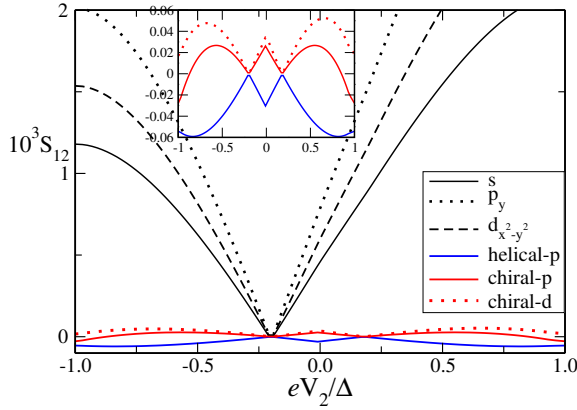


Figure 10: Shot noise cross-correlation ($10^3 S_{12}$) in units of $4|e|^2/h$ for $N_1/I/US/I/N_2$ junction vs bias voltage (eV_2/Δ) for different pairing symmetries with $k_F R = 100$, $R/\xi = 2$, $eV_1/\Delta = 0.2$ and $z = 0.1$ (Transparent barriers).

In Fig. 10, magnitude of shot noise cross-correlation in case of transparent barriers and for non-topological pairing is almost 100 times larger than topological pairing. Shot noise cross-correlation for helical- p pairing is negative for entire range of bias voltage ($-1 < eV_2/\Delta < 1$) and shows ZBP. Shot noise cross-correlations are completely positive in entire range of bias voltage ($-1 < eV_2/\Delta < 1$) for chiral- d superconductors while for chiral- p superconductors they turn negative when $eV_2 \rightarrow \pm\Delta$. When $V_2 = V_1$, shot noise cross-correlation for topological superconductors (both helical- p and chiral- p and

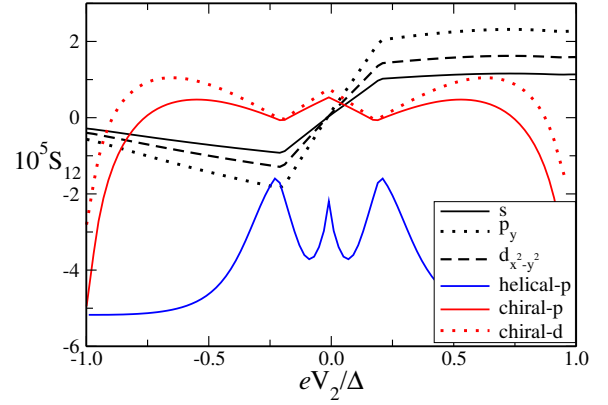


Figure 11: Shot noise cross-correlation ($10^5 S_{12}$) in units of $4|e|^2/h$ for $N_1/I/US/I/N_2$ junction vs bias voltage (eV_2/Δ) for different pairing symmetries with $k_F R = 100$, $R/\xi = 2$, $eV_1/\Delta = 0.2$ and $z = 3$ (Tunnel barriers).

d) are zero, but it is finite for non-topological superconductors (s , p_y and $d_{x^2-y^2}$). When $V_2 = \pm V_1$, shot noise cross-correlations for topological-superconductors (chiral- p , d and helical- p) vanish. However, in case of non-topological superconductors (s , p_y and $d_{x^2-y^2}$) shot noise cross-correlations are positive for entire range of bias voltage ($-1 < eV_2/\Delta < 1$) and vanish only at $V_2 = -V_1$. Thus shot noise cross-correlations in transparent limit can be a good indicator of topological pairing.

In Fig. 11, shot noise cross-correlation for helical- p superconductor is negative for entire range of bias voltage ($-1 < eV_2/\Delta < 1$) and shows ZBP. For chiral superconductors (both p and d), shot noise cross-correlations show ZBP and change sign from positive to negative when $eV_2 \rightarrow \pm\Delta$. When $V_2 \rightarrow \pm V_1$, shot noise cross-correlations for helical- p superconductor is negative and shows a dip while for chiral superconductors (both p and d) it is positive and shows a dip. Shot noise cross-correlation for non-topological superconductors (s , p_y and $d_{x^2-y^2}$) is negative for negative applied bias voltage ($-1 < eV_2/\Delta < 0$) and positive for positive applied bias voltage ($0 < eV_2/\Delta < 1$), thus in the entire bias voltage range $-V_1 < V_2 < V_1$, shot noise cross-correlations for non-topological superconductors (s , p_y and $d_{x^2-y^2}$) linearly increases as function of V_2 . For topological superconductors, on the other hand, shot noise cross correlations even though symmetric with respect to reversal in bias voltage V_2 , show non-linear behaviour as function of V_2 .

D. Processes at play

Shot noise cross-correlations have been calculated in metal/superconductor/metal hybrid junctions to study Cooper pair splitting, see Refs. [34, 44, 51]. Shot noise cross-correlations for s -wave superconductor show linear behaviour ($\propto V_2$) in bias voltage range ($-V_1 < V_2 < V_1$) which has been predicted in Refs. [44, 51–53] and also explained in Ref. [34].

Shot noise cross-correlations vanish at $V_2 = -V_1$ in transparent limit which has also been predicted in Ref. [52]. In the subsections below, we try to understand the reasons for the plots shown in Fig. 10 (transparent limit) and Fig. 11 (tunnel limit).

1. Tunnel limit

Shot noise cross-correlations, from Eq. 15 of Appendix, consists of local (AR-Andreev reflection, NR-normal reflection) amplitudes and non-local (CAR, EC) amplitudes. Each term in shot noise cross-correlation given in Eq. 15 consists of four amplitudes which can be grouped as EC-NR, CAR-NR, EC-AR, CAR-AR and also a mixed group of all four processes. EC-NR implies product of elastic cotunneling amplitudes and normal reflection amplitudes, such as $s_{12}^{ee}s_{21}^{ee}s_{22}^{ee*}s_{11}^{ee*}$, similarly CAR-NR is product of crossed Andreev reflection amplitudes and normal reflection amplitudes, such as $s_{21}^{eh}s_{12}^{he}s_{11}^{hh*}s_{22}^{ee*}$, CAR-AR is product of crossed Andreev reflection amplitudes and Andreev reflection amplitudes, such as $s_{21}^{he}s_{12}^{he}s_{11}^{he*}s_{22}^{ee*}$ and EC-AR is product of elastic cotunneling amplitudes and Andreev reflection amplitudes, such as $s_{21}^{he}s_{12}^{he}s_{11}^{hh*}s_{22}^{ee*}$. As NR amplitudes (s_{11}^{hh}, s_{22}^{ee}) $\rightarrow 1$ in tunnel limit for large z , hence, CAR-NR terms in S_{12} reduces to just CAR (or $s_{CAR} = s_{21}^{eh}s_{12}^{he}$) and EC-NR reduces to just EC, (or $s_{EC} = s_{12}^{ee}s_{21}^{ee}$). S^{EC} contribution to shot noise cross-correlations in tunnel limit, using electron hole symmetry in scattering matrix amplitudes gives $S^{EC} = s_{EC}(h_1 + h_2)$, where h_1, h_2 are Heaviside theta function and given in Eq. 15, while S^{CAR} contribution to shot noise cross-correlations in tunnel limit, which again using electron hole symmetry gives $S^{CAR} = s_{CAR}(h_3 + h_4)$, where h_3, h_4 are given in Eq. 15. Shot noise cross-correlations in tunnel limit in small bias voltage regime ($-V_1 < V_2 < V_1$) can be written as $S^{12} = S^{CAR} + S^{EC}$, with $S^{EC} = (s_{12}^{ee}s_{21}^{ee})(\Theta(e|V_1 - E) - \Theta(e|V_2 - E) - \Theta(-e|V_1 - E) + \Theta(-e|V_2 - E))$ and $S^{CAR} = (s_{21}^{eh}s_{12}^{he})(-\Theta(e|V_1 - E) - \Theta(e|V_2 - E) + \Theta(-e|V_1 - E) + \Theta(-e|V_2 - E))$, where Θ is Heaviside theta function.

This analysis for tunnel limit holds true for non-topological (s , p_y and $d_{x^2-y^2}$) as well as chiral (both p and d) superconductors. However, for helical- p pairing, NR amplitudes (s_{11}^{hh}, s_{22}^{ee}) $\nrightarrow 1$ in tunnel limit. Thus, S^{CAR-NR} does not reduce to S^{CAR} and S^{EC-NR} does not reduce to S^{EC} . Therefore for helical- p , $S^{12} = S^{CAR-NR} + S^{EC-NR}$, where $S^{CAR-NR} = (s_{21}^{eh}s_{12}^{he}s_{11}^{hh*}s_{22}^{ee*})(h_3 + h_4)$ and $S^{EC-NR} = (s_{12}^{ee}s_{21}^{ee}s_{11}^{hh*}s_{22}^{ee*})(h_1 + h_2)$.

From Fig. 12, it is clear that CAR contribution gives rise to positive shot noise cross-correlations whereas EC contribution gives rise to negative shot noise cross-correlations in the tunnel limit for both non-topological and chiral pairings, whereas for helical- p pairing both CAR-NR and EC-NR contributions gives rise to negative cross-correlations, as finite NR contributions are present

In Fig. 12, red lines are for S^{CAR} contribution which dominates for positive bias ($V_1, V_2 > 0$) and vanishes at $V_2 = -V_1$ for non-topological superconductors, whereas orange lines are for S^{EC} contribution which dominates when bias voltages are

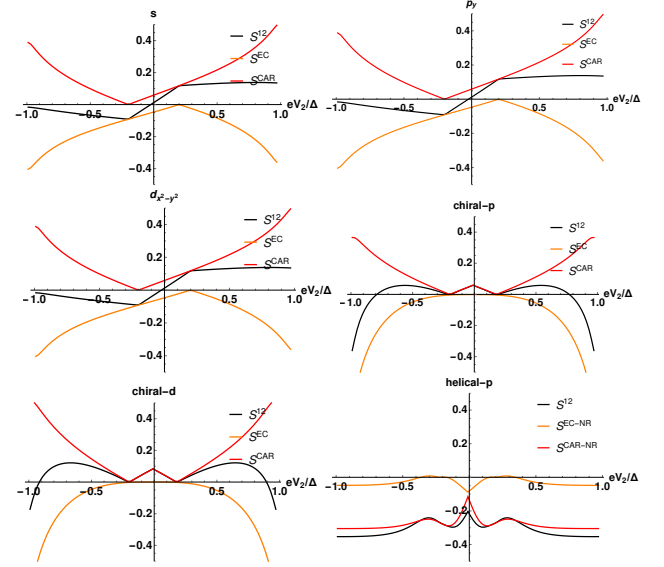


Figure 12: Shot noise cross-correlations in units of $(10^4) 4e^2/h$ for $N_1/I/US/I/N_2$ junction vs bias voltage (eV_2/Δ) for non-topological and topological superconductors with $k_F R = 100$, $R/\xi = 2$, $eV_1/\Delta = 0.2$ and $z = 3$ (tunnel barriers) for S^{CAR} (red line), S^{EC} (orange line) and S^{12} (black line). Note: $S^{12} = S^{CAR} + S^{EC}$ for non-topological and chiral cases but $S^{12} = S^{CAR-NR} + S^{EC-NR}$ for helical- p case.

of opposite sign (i.e., V_2 is negative and V_1 is positive or vice versa) and vanishes at $V_2 = V_1$. In Fig. 12, for chiral (both p and d) superconductors S^{CAR} contribution dominates for small bias voltage for both positive as well as negative bias voltages, while S^{EC} contribution vanishes for small bias voltage. When $eV_2 \rightarrow \Delta$, S^{EC} contribution dominates which leads to change in sign from positive to negative shot noise cross-correlations. For chiral superconductors, S^{CAR} contributions vanish at $V_2 = \pm V_1$ unlike non-topological superconductors whereas S^{CAR} contributions vanish only at $V_2 = -V_1$.

As predicted in Ref. [51] the shot noise cross-correlations for s wave superconductor in tunnel limit for small bias voltages at zero temperature reduces to

$$S_{tunnel}^{12}(\text{non-topological}) \propto eV_2. \quad (11)$$

It holds only for non-topological superconductors. Shot noise cross-correlations for topological chiral and helical- p superconductors in tunnel limit for small bias voltages are given as

$$S_{tunnel}^{12}(\text{chiral}) \propto eV_1 - |eV_2|, \\ S_{tunnel}^{12}(\text{helical-p}) \propto eV_1 - |eV_2| - c, \quad (12)$$

where c is constant term in helical- p case, comes from negative S^{CAR-NR} contributions to shot noise cross correlations. For topological superconductor, shot noise cross-correlations in tunnel limit is symmetries with respect to bias voltage

(V_2). In small bias voltage regime $-V_1 < V_2 < V_1$, shot noise cross correlations for non-topological superconductors (s , p_y , $d_{x^2-y^2}$) in tunnel limit shows linear behaviour as function of bias voltage V_2 as also seen for s -wave case. Shot noise cross-correlations predicted in our work for non-topological superconductors are in line with that seen for s wave superconductor in Refs. [51, 52].

2. Transparent limit

From Ref. [34], for s -wave, shot noise cross-correlations in transparent limit has only EC-AR contribution. Shot noise cross-correlations for all pairing symmetries in transparent limit ($z = 0.0$) gives EC-AR contribution to transport and is given as $S^{12} = S^{EC-AR} = s_{EC-AR} h_{EC-AR}$, where $s_{EC-AR} = s_{12}^{ee} s_{11}^{eh*} s_{21}^{hh} s_{22}^{he*}$ and $h_{EC-AR} = h_3 + h_4$, where h_3 and h_4 are Heaviside theta functions given in Eq. 15. In simplified form shot noise cross-correlations in transparent limit ($z = 0.0$) for small bias voltage regime $-V_1 < V_2 < V_1$ is $S^{12} = S^{EC-AR} = (s_{12}^{ee} s_{11}^{eh*} s_{21}^{hh} s_{22}^{he*}) (-\Theta(e|V_1 - E) - \Theta(e|V_2 - E) + \Theta(-e|V_1 - E) + \Theta(-e|V_2 - E))$, where Θ is Heaviside theta function. In the transparent limit S^{EC-AR} contribution to shot noise cross-correlations dominates for all pairings as plotted in Fig. 13 which vanish at $V_2 = -V_1$ for non-topological case as given in Eq. 13 and for topological case vanish at $V_2 = \pm V_1$.

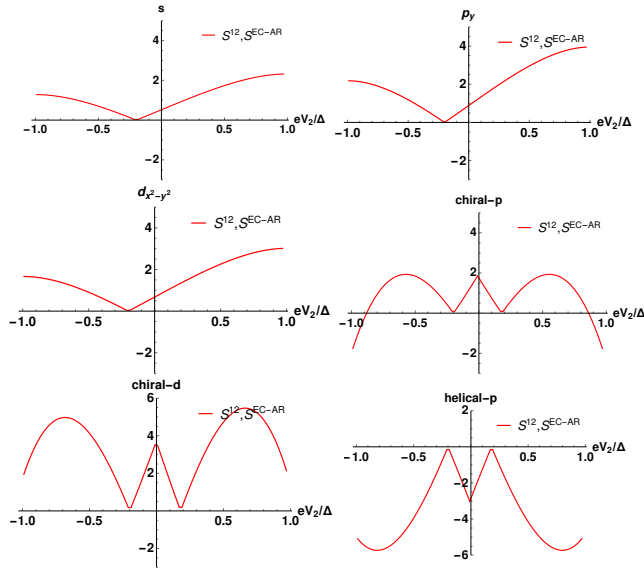


Figure 13: Shot noise cross-correlations in units of $4e^2/h$ for $N_1/I/US/I/N_2$ junction vs bias voltage (eV_2/Δ) for non-topological superconductors ($\times 10^3$) and topological superconductors ($\times 10^5$) with $k_F R = 100$, $R/\xi = 2$, $eV_1/\Delta = 0.2$ and $z = 0.0$ (transparent limit) for S^{EC-AR} and S^{12} (red line). The plot for S^{EC-AR} contribution and S^{12} overlap exactly.

In Fig. 13, S^{EC-AR} contribution to shot noise cross-

correlations changes sign from positive to negative only for chiral- p superconductor and is negative throughout for helical- p superconductor. Shot noise cross-correlations for all pairing symmetries in Fig. 13 shown for $z = 0.0$ (transparent limit) shows similar behaviour as shown in Fig. 10 for $z = 0.1$. As predicted in Ref. [52], shot noise cross-correlations for s -wave superconductor in transparent limit at zero temperature reduces to,

$$S_{transparent}^{12}(\text{non-topological}) \propto (eV_1 + eV_2). \quad (13)$$

It only holds for non-topological superconductors. For topological superconductors, shot noise cross-correlations in transparent limit can be written as,

$$S_{transparent}^{12}(\text{topological}) \propto \delta(eV_1 - |eV_2|), \quad (14)$$

where $\delta = +1$, for chiral case and $\delta = -1$, for helical- p case. Bias voltage dependence of shot noise cross-correlations for chiral pairing is same for both transparent as well as tunnel limit, whereas for helical- p pairing, barrier strength has an influence on bias voltage dependence of shot noise cross-correlations.

We have observed that shot noise cross-correlations for topological superconductors do not obey the linearity in bias voltage V_2 because of the difference in pairing symmetry and θ dependence in \mathbf{d} which is due to nontrivial topology that is pivotal in distinguishing various topological pairing and also the reason for SABS.

V. EXPERIMENTAL REALIZATION & CONCLUSION

Experiments on NSN junctions, similar to that shown in Fig. 2, but with s -wave superconductors are already a decade old. In Ref. [54], positive shot noise crosscorrelations were experimentally observed for the first time in a NSN junction with Copper being the metal and Aluminium as a s -wave superconductor. Next in Ref. [55], when Gold replaced Copper as the metal in NSN junction, similar positive shot noise cross-correlations were again seen. Uniquely, in Ref. [55], effects of an external magnetic field on shot noise cross correlations were also taken into account. Finally, in a more recent experiment, shot noise auto correlations were measured in a Metal-High T_c cuprate superconductor junction[56]. Extending these experimental setups to metal-topological superconductor-metal junctions and then measuring shot noise cross correlations should reveal the signatures of the distinct pairing symmetries.

Our main motivation is to distinguish the pairing symmetry of topological superconductor using shot noise cross-correlations in both symmetric as well as non-local setups of metal/superconductor/metal hybrid junction. G_{CAR} and G_{EC} for helical- p superconductors tend to finite values in the tunnel limit ($z \rightarrow \text{large}$) while for all other cases in tunnel limit both G_{CAR} and G_{EC} vanish. In Table II, we summarize the results of our work, with respect to differential non-local conductance and differential shot noise cross-correlation in both symmetric as well as non-local setups. When $eV_1 \rightarrow \pm\Delta$, G_{NL} for

helical- p superconductor shows a ZBP while for chiral superconductors (both chiral- p and chiral- d) shows a ZBD and for non-topological superconductors it is flat throughout. Regardless of whether we take symmetric or non-local set up, differential shot noise cross-correlation for helical- p superconductor is negative in transparent limit ($z \rightarrow 0$) but for all other cases it is positive. Differential shot noise cross-correlation for helical- p superconductor, changes sign from negative to positive with increase in z . In both symmetric as well as non-local set up, differential shot noise cross-correlation for a helical- p superconductor shows ZBP and is negative for entire range of bias voltage while for non-topological superconductors it is positive for entire range of bias voltage. Differential shot noise cross-correlation for chiral superconductors (chiral- p and chiral- d) shows a ZBD and is completely negative for entire range of bias voltage in non-local set up, while in symmetric setup chiral- p turns positive at zero bias. Regardless of whether we consider symmetric or non-local set up, differential shot noise cross-correlation for helical- p superconductor is always negative in the transparent limit and for intermediate barrier strength for entire range of bias voltages, which is uniquely associated with helical- p pairing.

We sum up the results of shot noise cross-correlations in Table III. Regardless of whether one considers transparent limit ($z = 0.1$) or tunnel limit ($z = 3$), shot noise cross-correlations for helical- p superconductor are always negative for entire range of bias voltage ($-1 < eV_2/\Delta < 1$). In the tunnel limit, shot

noise cross-correlations for chiral superconductors (both p and d) change sign from positive to negative when $eV_2 \rightarrow \pm\Delta$. In the transparent limit, for a wide range of bias voltages both chiral- p and d show positive shot noise cross-correlations, however in the limit $eV_2 \rightarrow \pm\Delta$, shot noise cross-correlations for chiral- p change sign. Shot noise cross-correlation for non-topological superconductors are completely positive in the transparent limit ($z = 0.1$), however in the tunnel limit ($z = 3$) they change sign as a function of applied bias voltage V_2 . For bias voltage in the range $-V_1 < V_2 < V_1$, shot noise cross-correlations for non-topological superconductors are $\propto V_2$ in the tunnel limit while for topological superconductor are $\propto V_1 - |V_2|$ as shown in Section IV. D.

Our approach using non-local differential conductance, differential shot noise cross-correlation and shot noise cross-correlation to probe both chiral- p , chiral- d as well as helical- p pairing in topological superconductors will be helpful in distinguishing clearly helical from chiral pairing, unlike Knight shift measurement that does not resolve the helical and chiral dichotomy. Our method will give an easy way for experimentalists to distinguish non-topological superconductors from both chiral- p , chiral- d as well as helical- p superconductors via using differential shot noise cross-correlation and shot noise cross-correlation. In future we will extend our study to probe topological character of superconducting Dirac materials using shot noise cross-correlations.

Table II: Properties of G_{NL} and differential shot noise cross-correlation in $N_1/I/US/I/N_2$ junction.

Topology	Type	Pairing	Differential non-local conductance		Differential shot noise cross-correlation							
					Symmetric set up		Non-local set up		Symmetric set up		Non-local set up	
			$z = 1, eV_2/\Delta = 0$		$z = 1, eV_1 = eV_2$		$z = 1, eV_2/\Delta = 0$		$eV_1/\Delta = eV_2/\Delta = 0.2$		$eV_1/\Delta = 0.2, eV_2/\Delta = 0$	
			$eV_1/\Delta = 0$	$eV_1 = \pm\Delta$	$eV_1/\Delta = 0$	$eV_1 = \pm\Delta$	$eV_1/\Delta = 0$	$eV_1 = \pm\Delta$	Transparent	Tunneling	Transparent	Tunneling
Non Topological	Gapful	s	Flat, Negative	Vanishing	Flat, Positive	Vanishing	Flat, Positive	Vanishing	Positive	Vanishing	Positive	Vanishing
	Nodal	p_y	Flat, Negative	Vanishing	Flat, Positive	Positive	Flat, Positive	Positive	Positive	Vanishing	Positive	Vanishing
		$d_{x^2-y^2}$	Flat, Negative	Vanishing	Flat, Positive	Positive	Flat, Positive	Positive	Positive	Vanishing	Positive	Vanishing
Topological	Chiral (Gapful)	$p_x + ip_y$	ZBD, Negative	Negative	ZBD, Positive	Negative	ZBD, Negative	Negative	Positive	Vanishing	Positive	Vanishing
		$d_{x^2-y^2} + id_{xy}$	ZBD, Negative	Negative	ZBD, Negative	Negative	ZBD, Negative	Negative	Positive	Vanishing	Positive	Vanishing
	Helical (Gapful)	p	ZBP, Negative	Vanishing	ZBP, Negative	Vanishing	ZBP, Negative	Vanishing	Negative	Positive	Negative	Negative

VI. APPENDIX: SHOT NOISE CROSS-CORRELATION

In this appendix we give the detailed expression for shot noise cross-correlation. Shot noise cross-correlation as given in

Eq. 2 can be simplified as

$$S_{12} = \frac{4e^2}{h} \int_{-\pi/2}^{\pi/2} d\theta \frac{\cos\theta}{2\pi} \int dE \{ (s_1 + s_2)h_1 + (s_3 + s_4)h_2 + (s_5 + s_6)h_3 + (s_7 + s_8)h_4 + s_9h_5 + s_{10}h_6 + s_{11}h_7 + s_{12}h_8 + s_{13}h_9 + s_{14}h_{10} \}, \quad (15)$$

Table III: Properties of shot noise cross-correlation in $N_1/I/US/I/N_2$ junction.

Topology	Type	Pairing	Shot noise cross-correlation ($eV_1/\Delta = 0.2$)							
			Transparent limit ($z \rightarrow 0$)				Tunnel limit ($z \rightarrow large$)			
			$eV_2/\Delta \rightarrow 0$	$eV_2 = \pm\Delta$	$V_2 = V_1$	$-V_1 < V_2 < V_1$	$eV_2/\Delta \rightarrow 0$	$eV_2 = -\Delta$	$eV_2 = \Delta$	$-V_1 < V_2 < V_1$
Non topological	Gapful	s	Positive	Positive	Finite, Positive	$eV_1 + eV_2$	Vanishing	Vanishing, Negative	Vanishing, Positive	eV_2
	Nodal	p_y	Positive	Positive	Finite, Positive	$eV_1 + eV_2$	Vanishing	Negative	Positive	eV_2
		$d_{x^2-y^2}$	Positive	Positive	Finite, Positive	$eV_1 + eV_2$	Vanishing	Negative	Positive	eV_2
Topological	Chiral (Gapful)	$p_x + ip_y$	ZBP, Positive	Negative	Zero	$eV_1 - eV_2 $	ZBP, Positive	Negative	Negative	$eV_1 - eV_2 $
		$d_{x^2-y^2} + id_{xy}$	ZBP, Positive	Positive	Zero	$eV_1 - eV_2 $	ZBP, Positive	Negative	Negative	$eV_1 - eV_2 $
	Helical (Gapful)	p	ZBP, Negative	Negative	Zero	$-(eV_1 - eV_2)$	ZBP, Negative	Negative	Negative	$eV_1 - eV_2 - c$

where $s_1 = \mathbb{R}\{s_{12}^{ee} s_{11}^{ee*} s_{21}^{ee} s_{22}^{ee*}\}$, $s_2 = \mathbb{R}\{s_{21}^{he} s_{11}^{he*} s_{12}^{he} s_{22}^{he*}\}$, $s_3 = \mathbb{R}\{s_{12}^{hh} s_{11}^{hh*} s_{21}^{hh} s_{22}^{hh*}\}$, $s_4 = \mathbb{R}\{s_{12}^{eh} s_{11}^{eh*} s_{21}^{eh} s_{22}^{eh*}\}$, $s_5 = \mathbb{R}\{s_{21}^{eh} s_{11}^{eh*} s_{12}^{eh} s_{22}^{eh*}\}$, $s_6 = \mathbb{R}\{s_{12}^{ee} s_{11}^{ee*} s_{21}^{ee} s_{22}^{ee*}\}$, $s_7 = \mathbb{R}\{s_{12}^{eh} s_{11}^{eh*} s_{21}^{eh} s_{22}^{eh*}\}$, $s_8 = \mathbb{R}\{s_{12}^{hh} s_{11}^{hh*} s_{21}^{hh} s_{22}^{hh*}\}$, $s_9 = \mathbb{R}\{s_{12}^{eh} s_{11}^{eh*} s_{21}^{eh} s_{22}^{eh*} + s_{12}^{hh} s_{11}^{hh*} s_{21}^{hh} s_{22}^{hh*}\}$, $s_{10} = \mathbb{R}\{s_{12}^{ee} s_{11}^{ee*} s_{21}^{ee} s_{22}^{ee*} + s_{12}^{eh} s_{11}^{eh*} s_{21}^{eh} s_{22}^{eh*}\}$, $s_{11} = \mathbb{R}\{s_{12}^{ee} s_{11}^{ee*} s_{21}^{eh} s_{22}^{eh*} + s_{12}^{eh} s_{11}^{eh*} s_{21}^{ee} s_{22}^{ee*}\}$, $s_{12} = \mathbb{R}\{s_{12}^{eh} s_{11}^{eh*} s_{21}^{ee} s_{22}^{ee*} + s_{12}^{hh} s_{11}^{hh*} s_{21}^{hh} s_{22}^{hh*}\}$, $s_{13} = \mathbb{R}\{s_{11}^{ee} s_{12}^{ee*} s_{21}^{eh} s_{22}^{eh*} + s_{11}^{hh} s_{12}^{hh*} s_{21}^{eh} s_{22}^{eh*}\}$, $s_{14} = \mathbb{R}\{s_{12}^{ee} s_{11}^{ee*} s_{21}^{eh} s_{22}^{eh*} + s_{12}^{hh} s_{11}^{hh*} s_{21}^{eh} s_{22}^{eh*} - s_{12}^{eh} s_{11}^{eh*} s_{21}^{ee} s_{22}^{ee*} - s_{12}^{hh} s_{11}^{hh*} s_{21}^{ee} s_{22}^{ee*}\}$. Fermi function as given in Eq. 2 for electron

and hole in contact i are $f_{ie}(E) = \left[1 + \exp\left(\frac{E - |eV_i|}{k_B T}\right)\right]^{-1}$

and $f_{ih}(E) = \left[1 + \exp\left(\frac{E + |eV_i|}{k_B T}\right)\right]^{-1}$, where k_B is Boltzmann constant and T is temperature. At zero temperature, $f_{ie}(E) \rightarrow \Theta(|eV_i| - E)$ and $f_{ih}(E) \rightarrow \Theta(|eV_i| + E)$, where Θ is Heaviside theta function. Heaviside theta function components of shot noise cross-correlation given in Eq. 15 are

$h_1 = \Theta(|eV_1| - E) - 2\Theta(|eV_1| - E)\Theta(|eV_2| - E) + \Theta(|eV_2| - E)$, $h_2 = \Theta(-|eV_1| - E) - 2\Theta(-|eV_1| - E)\Theta(-|eV_2| - E) + \Theta(-|eV_2| - E)$, $h_3 = -\Theta(-|eV_1| - E) + 2\Theta(-|eV_1| - E)\Theta(|eV_2| - E) - \Theta(|eV_2| - E)$, $h_4 = -\Theta(|eV_1| - E) + 2\Theta(|eV_1| - E)\Theta(-|eV_2| - E) - \Theta(-|eV_2| - E)$, $h_5 = -\Theta(-|eV_1| - E) + 2\Theta(-|eV_1| - E)\Theta(-|eV_2| - E) - \Theta(-|eV_2| - E)$, $h_6 = -\Theta(|eV_1| - E) + 2\Theta(|eV_1| - E)\Theta(|eV_2| - E) - \Theta(|eV_2| - E)$, $h_7 = \Theta(-|eV_1| - E) - 2\Theta(-|eV_1| - E)\Theta(|eV_2| - E) + \Theta(|eV_2| - E)$, $h_8 = \Theta(|eV_1| - E) - 2\Theta(|eV_1| - E)\Theta(-|eV_2| - E) + \Theta(-|eV_2| - E)$, $h_9 = \Theta(|eV_2| - E) - 2\Theta(|eV_2| - E)\Theta(-|eV_2| - E) + \Theta(-|eV_2| - E)$, $h_{10} = \Theta(|eV_1| - E) - 2\Theta(|eV_1| - E)\Theta(-|eV_1| - E) + \Theta(-|eV_1| - E)$.

VII. ACKNOWLEDGMENTS

This work was supported by funds from the grant "Josephson junctions with strained Dirac materials and their application in quantum information processing" from Science & Engineering Research Board (SERB), New Delhi, Government of India, under Grant No. CRG/2019/006258.

- [1] H. R. Ott, et. al., Phys. Rev. Lett. 52, 1915 (1984).
- [2] L. J. Buchholtz and G. Zwirnagl, Phys. Rev. B 23, 5788 (1981); C. Bruder, Phys. Rev. B 41, 4017 (1990).
- [3] M. S. Scheurer and J. Schmalian, Nature communications 6, 6005 (2015); S. D. Sarma, C. Nayak and S. Tewari, Phys. Rev. B 73, 220502 (2006).
- [4] J. Alicea, Rep. Prog. Phys. 75, 076501 (2012); C.W.J. Beenakker, Rev. Condens. Matter Phys. 4, 113-136 (2013).
- [5] K. K. Tanaka, M. Ichioka and S. Onari, Journal of Physics: Conf. Series 871, 012024 (2017); H. Hu, I. I. Satija and E. Zhao, arXiv:1812.05014 (2018).
- [6] M. Sato, et. al., Phys. Rev. B 83, 224511 (2011).
- [7] Shun Tamura, et. al., Phys. Rev. B 95, 104511 (2017).

- [8] X. L. Qi, T. L. Hughes and S. C. Zhang, Phys. Rev. B 81, 134508 (2010); E. F. Dumitrescu, Majorana fermions in chiral topological superconductors, Ph.D. thesis, Clemson University (Dec 2014).
- [9] C. Xu and J. E. Moore, Phys. Rev. B 73, 045322 (2006); T. H. Hsieh and L. Fu, Phys. Rev. Lett 108, 107005 (2012).
- [10] S. Ikegaya, et. al., arXiv:1912.13250v1 (2019).
- [11] A. P. Schnyder, et. al., Phys. Rev. B 78, 195125 (2008).
- [12] Isil Ozfidan, Jinsen Han and Joseph Maciejko, Phys. Rev. B 94, 214510 (2016).
- [13] A. J. Leggett and Y. Liu, arXiv:2010.15220v1 (2020).
- [14] Ishida K, et. al., Nature 396 (1998); A.J. Leggett, Phys. Rev. Lett. 14, 536 (1965); H. Mukuda, et. al., Phys. Soc. Jpn. 67, 3945 (1998).

- [15] R. Jin, et. al., EPL 51, 341 (2000).
- [16] S. Kashiwaya, et. al., Phys. Rev. B 100, 094530 (2019).
- [17] K. Ishida, et. al., J. Phys. Soc. Jpn. 89, 034712 (2020).
- [18] J. R. Kirtley, et. al., Phys. Rev. B 76, 014526 (2007); C. W. Hicks, et. al., Phys. Rev. B 81, 214501 (2010).
- [19] S. Kashiwaya and Y. Tanaka, Rep. Prog. phys. 63, 1641 (2000).
- [20] P. Burset, et. al., Phys. Rev. B 95, 224502 (2017).
- [21] D. S. Manzano, et. al., arXiv:2009.03196.
- [22] Y. Tanaka and S. Kashiwaya, Phys. Rev. Lett. 74, 3451 (1995).
- [23] P. J. Churran, et. al., Phys. Rev. B 89, 144504 (2014).
- [24] S. Nakosai, Y. Tanaka, N. Nagosa, Phys. Rev. B 88, 180503 (2013).
- [25] Yusuke Nomura, et. al., Journal of Phys.: Condensed matter 28, 153001 (2016).
- [26] S. J. Sun, et. al., Scientific Reports 6, 24102 (2016); Y. Nishikubo, et. al., Journal of the Physical Society of Japan 80, 055002 (2011).
- [27] R. Hanbury Brown and R. Q. Twiss, Philosophical Magazine 45, 663 (1954); M. Rudolph and P. Heymann.
- [28] C. Kallin, J. Berlinsky, Rep. Prog. Phys. 79, 054502 (2016); A. P. Mackenzie, Y. Maeno, Rev. Mod. Phys. 75, 657 (2003).
- [29] J. Zhang, et. al., J. Phys.: Condens. Matter 26, 252201 (2014); Sigrist M and Ueda K, Rev. Mod. Phys. 63, 239 (1991); A. P. Mackenzie and Y. Maeno, Physica B 280, 148 (2000).
- [30] N. A. Mortensen, K. Flensberg and A. P. Jauho, Phys. Rev. B 59, 10176 (1999).
- [31] K. Zhang and Q. Cheng, Supercond. Sci. Technol. 31, 075001 (2018).
- [32] G. E. Blonder, M. Tinkham and T. M. Klapwijk, Phys. Rev. B 25, 4515 (1982).
- [33] C. Benjamin, J. K. Pachos, Phys. Rev. B 78, 235403 (2008).
- [34] M. Floser, D. Feinberg and R. Melin, Phys. Rev. B 88, 094517 (2013); Martina Flöser, Transport local et non-local: Percolation dans les systemes a effet Hall quantique correlations croisees dans les structures hybrides supraconductrices, University de Grenoble, Doctoral thesis (2012).
- [35] M. P. Anantram and S. Datta, Phys. Rev. B 53, 16390 (1996).
- [36] M. J. M. de Jong and C. W. J. Beenakker, Phys. Rev. Lett. 74, 1657 (1995); M. J. M. de Jong and C. W. J. Beenakker, Phys. Rev. B 49, 16070(R) (1994).
- [37] Z. C. Dong, et. al., J. Phys.:Condens. Matter 13, 3839.
- [38] C. Beenakker and C. Schönenberger, Physics Today May 2003, p. 37.
- [39] Y. M. Blanter and M. Buttiker, Phys. Rep. 336, 1 (2000).
- [40] S. Mi, P. Burset and C. Flindt, Sci. Rep. 8, 16828 (2018).
- [41] P. Burset, et. al., Phys. Rev. B 90, 085438 (2014); C. Kallin, Rep. Prog. Phys. 75, 042501 (2012).
- [42] Q. Cheng, B. jin and D. Yu, Physics letters A 379, 1172 (2015); Y. Tanaka, et. al., Phys. Rev. B 79, 060505 (2009).
- [43] S. Zhang and B. Trauzettel, Phys. Rev. Lett. 122, 257701 (2019).
- [44] R. Melin, C. Benjamin and T. Martin, Phys. Rev. B 77, 094512 (2008).
- [45] R. Melin and D. Feinberg, Phys. Rev. B 70, 174509 (2004).
- [46] Z. Dong and H. Fu, Sci China Ser G: Phy & Ast 47, 256–264 (2004).
- [47] W. Liming, et. al., Front. of Phys. 10, 1007 (2012).
- [48] Y. Liu and Z. Q. Mao, Physica C 514, 339 (2015); A. P. Mackenzie, et. al., Phys. Rev. Lett. 80, 161 (1998).
- [49] X. Wu and H. Meng, The European Physical Journal B 88, 128 (2015).
- [50] Z. C. Dong, et. al., Phys. Rev. B 67, 134515 (2003).
- [51] G. Bignon, M. Houzet, F. Pistolesi, and F. W. J. Hekking, Europhys. Lett. 67, 110 (2004).
- [52] D. S. Golubev and A. D. Zaikin, Phys. Rev. B 99, 144504 (2019).
- [53] A. V. Bubis, et. al., arXiv: 2101.10343v1.
- [54] J. Wei and V. Chandrasekhar, Nature Physics 6, 494 (2010);
- [55] A. Das, et. al., Nature Comms. 3, 1165 (2012).
- [56] K. M. Bastiaans, et. al., Nature Physics 14, 1183 (2018).